# URANS simulation of flow over smooth topography

A. Nakayama and K. Miyashita
*Graduate School of Science and Technology, Kobe University, Kobe, Japan*

Received October 2000
Revised July 2001
Accepted July 2001

***Keywords*** *Flow production, Model, Simulation*

***Abstract*** *An Unsteady Reynolds-Averaged Navier-Stokes (URANS) equation method has been applied to compute the flow over two-dimensional smooth topography and compared with conventional RANS and large-eddy simulation (LES) results. The URANS calculation with sufficient grid resolution near solid surface and an appropriate near-wall model has been shown to simulate much of the large-scale unsteadiness and some of the turbulent motion for flows with and without separation. Although the results with unadjusted model constants do not show an overwhelming improvement over a standard two-equation model, it is demonstrated that it may be improved and, more importantly, can be generalized to a new simulation technique by refining the model, considering such factors as grid-dependent length scales and by making a three-dimensional calculation.*

## 1. Introduction

While direct numerical simulations (DNS) are giving important information on mechanisms of turbulence at low Reynolds numbers, even LES of a sufficient resolution still is difficult in most engineering applications and there still is much expectation on the methods based on Reynolds averaged equations. Reynolds-averaged Navier-Stokes (RANS) equation methods are intended to solve for Reynolds-averaged flows and if the boundary conditions are time-independent, the solution should be a steady flow, even if a time-marching calculation is performed. When there is a periodic large-scale unsteadiness in the flow, such as the case of vortex shedding off bluff bodies, the unsteady RANS equations may be considered to represent the phase-averaged flow and the time-dependent solution is conceivable (Rodi, 1993). Franke and Rodi (1991), Bosch and Rodi (1998), Shimada and Meng (1998) and Lee (1997) applied various RANS methods in unsteady forms to calculation of vortex-shedding flow past square and rectangular cylinders. Iaccarino and Durbun (2000) conducted a calculation of three-dimensional unsteady flow using a RANS technique. The degree of unsteadiness obtained by different calculation methods was found to depend on the turbulence model used and that it is the periodic unsteadiness of large-scale vortex shedding motion and no random turbulence was calculated. Conventional RANS calculations of separated flows over hills by Okajima *et al.* (1998), Ishihara (1999) and Ishihara and Hibi (2000), on the other hand, do not show any unsteadiness, even the periodic vortex shedding motion. These calculations employ relatively coarse grids that do not resolve the low-Reynolds number region near solid boundaries. In their recent calculation of flow around a square cylinder using a non-linear $k$-$\varepsilon$ model, however, Kimura and Hosoda (1999) show a little more than pure periodic

International Journal of Numerical Methods for Heat & Fluid Flow, Vol. 11 No. 8, 2001, pp. 723-743.

vortex shedding. According to Shimada and Ishihara's (1999) calculation of flow past square and rectangular cylinders, irregular fluctuations due to possible turbulence were seen in the lift and drag forces only when turbulence model was not used. Some irregularities in the wall pressure are seen in the URANS calculation of Iaccarino and Durbin (2000). Garuelle and Ducros (1999) used a one-equation URANS model in the calculation of a boundary layer and found that no unsteadiness. It is not quite clear if a straightforward extension of a conventional RANS method to an unsteady turbulent flow can capture turbulence. In two-dimensional version of LES, however, random motion is reproduced and recent calculation by Bouris and Bergeles (1999) even indicates that a 2-D LES reproduced turbulence better than a 3-D LES, since very fine motion near the wall can be resolved.

Koutmos and Mavridis (1997) recognized that URANS and LES equations are equivalent, and modeled the eddy viscosity as a sum of contributions from the deterministic turbulence by $k$-$\varepsilon$ model and that due to filtering effects of the numerical grid by Smagorinsky model. Spalart (1999) proposed a simulation method that tries to exploit a RANS model in an unsteady mode and attempted to combine a RANS model with LES. Baggett (1998) also is trying to merge a RANS and LES models to be applied to high Reynolds number flows with relatively coarse mesh. Furthermore, Speziale (1998) suggested that a generalized sub-grid model that is derived from a RANS model to be used to compute turbulent flows with wide range of grid resolution and the Reynolds number. If, however, a URANS calculation can capture some or much of the turbulence motion, it can become a new simulation method with a single turbulence model. In the present study, a URANS method based on the $k$-$\varepsilon$ model resolving the near-wall flow is applied to calculation of boundary layer flows over smooth topography, with and without flow separation, to examine if in fact a URANS calculation can reproduce turbulence. Conventional LES and steady RANS calculation using standard $k$-$\varepsilon$ model are separately applied in order to clarify the meaning of unsteady RANS calculation and to explore a possible generalization to a turbulence simulation technique.

## 2. Basic equations

The Reynolds-averaged equations of motion for incompressible flows are derived by either time averaging or ensemble averaging of the equations for the instantaneous flows. The same equations are obtained by other averaging operations like a short-time averaging or spatial filtering, and for that matter, any linear operation that can commute with time and spatial differentiation. In the present context we avoid the precise definition of the averages and we consider the averaged quantities, denoted by $\langle\ \rangle$, that satisfy the unsteady Reynolds averaged equations of motion:

$$\frac{\partial\langle u_i\rangle}{\partial t} + \langle u_j\rangle\frac{\partial\langle u_i\rangle}{\partial x_j} = -\frac{1}{\rho}\frac{\partial\langle p\rangle}{\partial x_i} + \frac{\partial}{\partial x_j}\left(R_{ij} + \nu\frac{\partial\langle u_i\rangle}{\partial x_j}\right) \quad (1)$$

and the continuity equation:

$$\frac{\partial \langle u_i \rangle}{\partial x_i} = 0. \tag{2}$$

Here $u_i$ is the local instantaneous velocity component in $x_i$ direction, $p$ is the instantaneous pressure, $\nu$ and $\rho$ are the fluid kinematic viscosity and density, $R_{ij} = -\langle u_i u_j \rangle + \langle u_i \rangle \langle u_j \rangle$ is the added stress that arises from averaging of the nonlinear terms. Though the physical meaning of $R_{ij}$ and its method of modeling depend on the precise definition of the average, the conventional isotropic eddy viscosity representation:

$$R_{ij} = \frac{1}{3} R_{kk} \delta_{ij} - \nu_t \left( \frac{\partial \langle u_i \rangle}{\partial x_j} + \frac{\partial \langle u_j \rangle}{\partial x_i} \right) \tag{3}$$

where $\nu_t$ is the eddy viscosity coefficient, is one method of closure. Furthermore, if we use $\langle k \rangle$ to denote the kinetic energy of the fluctuation from the average $\langle u_i \rangle$, defined by $\langle k \rangle = -\frac{1}{2} R_{ii} = \frac{1}{2} (\langle u_i u_i \rangle - \langle u_i \rangle \langle u_i \rangle)$, and $\langle \varepsilon \rangle$ its rate of dissipation, we can follow $k$-$\varepsilon$ type two-equation turbulence model and represent $\nu_t$ by:

$$\nu_t = C_\mu \langle k \rangle^2 / \langle \varepsilon \rangle \tag{4}$$

with the value of the constant $C\mu$ expected to take the standard value of 0.09 at least when or in the limit the average approaches the long time average. Depending on the precise meaning of the averaging that we are inferring, it may not be quite the same as those implied by the conventional $k$-$\varepsilon$ model, but there should be no reason not to use the conventional model equations for solving these quantities:

$$\frac{\partial \langle k \rangle}{\partial t} + \langle u_j \rangle \frac{\partial \langle k \rangle}{\partial x_j} = P_{\langle k \rangle} + \frac{\partial}{\partial x_j} \left( \left( \nu + \frac{\nu_t}{\sigma_k} \right) \frac{\partial \langle k \rangle}{\partial x_j} \right) - \langle \varepsilon \rangle \tag{5}$$

$$\frac{\partial \langle \varepsilon \rangle}{\partial t} + \langle u_j \rangle \frac{\partial \langle \varepsilon \rangle}{\partial x_j} = C_1 P_{\langle k \rangle} \frac{\langle \varepsilon \rangle}{\langle k \rangle} + \frac{\partial}{\partial x_j} \left( \left( \nu + \frac{\nu_t}{\sigma_\varepsilon} \right) \frac{\partial \langle \varepsilon \rangle}{\partial x_j} \right) - C_2 \frac{\langle \varepsilon \rangle^2}{\langle k \rangle} \tag{6}$$

where $p_{\langle k \rangle}$ is the production of $\langle k \rangle$

$$P_{\langle k \rangle} = R_{ij} \frac{\partial \langle u_i \rangle}{\partial x_j}. \tag{7}$$

We may also use, for now, the standard values of the model constants, $C\mu$, $C_1$, $C_2$, $\sigma_k$ and $\sigma_\varepsilon$ until a firm reason against it is found. We also make a modification to equation (4) to apply the model in the low-Reynolds number region near solid boundary and we adopt the two-layer type modification following the method of Lakehal and Rodi (1997). Hence equation (4) is replaced by:

$$\nu_t = C_\mu \langle k \rangle^{1/2} l_\mu \tag{8}$$

in the near wall region, $R_y = \langle k \rangle^{1/2} y_n / \nu < 2.6$, and equation (6) is replaced by:

$$\langle \varepsilon \rangle = \langle k \rangle^{3/2} / l_\varepsilon \tag{9}$$

where

$$l_\mu = C_l y_n f_\mu \ , \quad l_\varepsilon = C_l y_n \frac{1}{1 + 13.2/(C_l R_y)} \tag{10}$$

$$f_\mu = 1 - \exp\left(-\frac{R_y}{50.5}\right) \ , \quad C_l = \kappa C_\mu^{-3/4} \tag{11}$$

and $\kappa$ is the Karman constant. $\langle k \rangle$ is solved up the wall using equation (5) applying the boundary condition $\langle k \rangle = 0$. The length scales $l_\mu$ and $l_\varepsilon$ with damping by equation (11) provide modeling of low-Reynolds number effects. As they stand, these equations are identical to the conventional RANS equations but the unsteady terms are now included in the equations of motion and in the transport equations.

The basic equations for LES method that we consider for comparison purposes, are very similar, except that the meaning of the averaging is clear which is the spatial filtering, and the additive stress terms are the sub-grid stresses which we may denote by $\tau_{ij}$. We retain the notation $\langle \ \rangle$ to represent the spatially filtered flow quantities, then the eddy viscosity formula for the subgrid stress is:

$$\tau_{ij} \ = \ \frac{1}{3}\tau_{kk}\delta_{ij} - \nu_t \left( \frac{\partial \langle u_i \rangle}{\partial x_j} + \frac{\partial \langle u_j \rangle}{\partial x_i} \right) \tag{12}$$

where $\nu_t$ now is the sub-grid stress eddy viscosity coefficient. In the present calculation we make use of the Smagorinsky model for $\nu_t$ and $\tau_{kk}$:

$$\nu_t = f(y^+)(C_S \Delta)^2 \left[ \frac{\partial \langle u_i \rangle}{\partial x_j} \left( \frac{\partial \langle u_i \rangle}{\partial x_j} + \frac{\partial \langle u_j \rangle}{\partial x_i} \right) \right]^{1/2} , \quad \tau_{kk} = \frac{2\nu_t^2}{(C_k \Delta)^2} \ , \tag{13}$$

where $\Delta$ is the length scale associated with the grid spacing for which we take the geometric average of the grid spacings in three directions $\Delta = \sqrt[3]{\Delta_x \Delta_y \Delta_z}$, $C_k$ and $C_S$ are model constants for which we use the standard values $C_k = 0.94$ and $C_S = 0.13$, and $f(y^+)$ is the Van-Driest type damping function depending on the distance $y_n$ to the nearest wall and is:

$$f(y^+) = 1 - \exp(-y^+/25) \ , \quad y^+ = y_n u_\tau / \nu \tag{14}$$

where $u_\tau$ is the friction velocity. With the damping function the equations of motion can be integrated up to the ground and the non-slip condition can be

applied there. Since the grid used in the present calculation is not quite fine enough in some regions at the present Reynolds number, a separate calculation is made, for the purpose of comparison, by assuming a three-layer wall-function velocity profile at the first calculation point from the ground.

## 3. Computational cases

The above URANS and LES calculation methods have been applied to the flow over smooth two-dimensional topographies shown in Figure 1. These are the cases for which experimental data have been collected by Nakamura *et al.* (1998). The first case is an isolated hill defined by an analytic equation:

$$\frac{z}{H} = \frac{1}{1 + (x_1/1.1H)^4} \tag{15}$$

where $z$ is the elevation of the ground at horizontal position $x1$, and $H$ is the height of the hill. The second case is an ascending slope described by:

$$\frac{z}{H} = \begin{cases} \frac{1}{1+(x_1/1.1H)^4}, & \frac{x_1}{H} > 0 \\ 1 \quad , & \frac{x_1}{H} \geq 0 \end{cases} \tag{16}$$

For both cases the maximum slope angle is 45 degrees from the horizontal direction. For these smooth boundaries, the separation point is not forced and is an important element to be predicted by a simulation method. According to the experiment described below, the flow separates downstream of the isolated hill but no separation is seen over the ascending slope, and these two cases provide representative cases with separation and without separation.

## 4. Numerical method

Numerical methods used in the present URANS and LES calculations are not the same but not entirely different, either. The largest difference is in the computational grids. In URANS calculation, a boundary fitted curvilinear coordinates are used, while Cartesian coordinates are used in the LES calculation, in which case the boundary condition is applied at the grid point

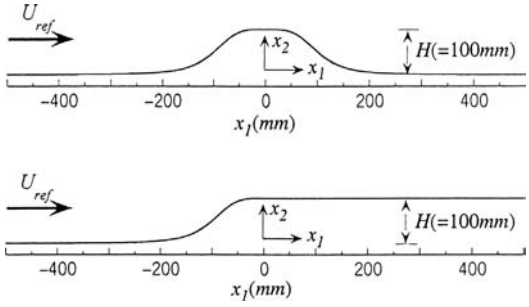


**Figure 1.**
Isolated hill and ascending slope models

closest to the boundary. The corresponding grids are shown in Figures 2 and 3. The grids used in URANS calculation are $150 \times 50$, covering the region $19H \times 10H$ in the streamwise and the vertical directions. The grids used in LES calculations are $123 \times 73 \times 20$, covering the three-dimensional region of $19H \times 10H \times 4H$. Both methods use the staggered mesh arrangement, the second-order finite differencing scheme for viscous and turbulence terms and third-order upwind differencing (UTOPIA) for the convective terms. MAC method is used for obtaining pressure in URANS method and HSMAC is applied in the LES computation. In both cases the momentum equations are integrated with time by an implicit Euler method, with the non-dimensional time step of 0.0001 starting from a uniform-flow initial condition. The present LES calculation is done using the same program as that used by Nakayama and Noda (2000), in which it is shown that the non-boundary fitting coordinate introduces errors similar to the linear extrapolation of velocity components near the boundary but does not induce any separation-like disturbances. We have also compared the calculations obtained by using boundary-fitted coordinates and rectangular coordinates, and verified that the small disturbance caused by the rectangular-grid approximation does not influence the mean velocity results of separating boundary layer over a smooth hill (Nakayama and Vengadesan, 2001).

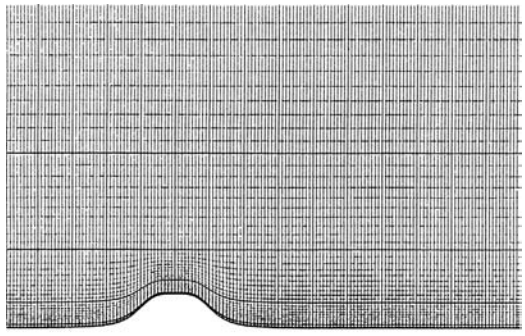

(a) grid for hill

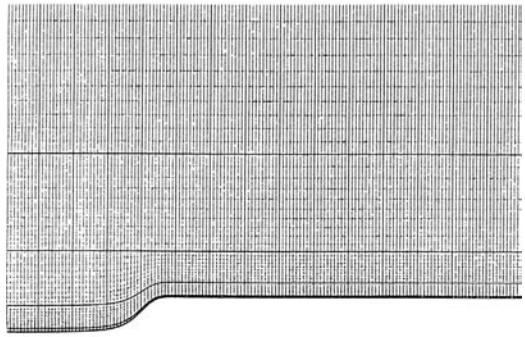

(b) grid for slope

**Figure 2.**
Computational grids used in URANS calculation

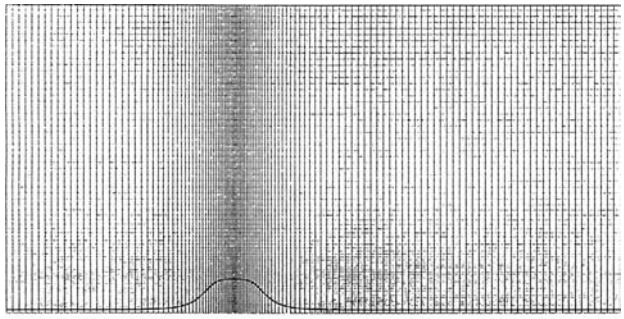

(a) grid for hill

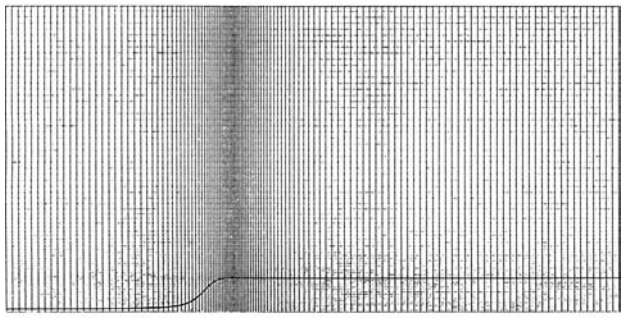

(b) grid for slope

**Figure 3.**
Computational grids ($123 \times 73 \times 20$) used in LES calculations

## 5. Summary of experiments

Experiments were carried out in a blower-type low-speed, low-turbulence (0.2 percent) wind tunnel of test section of 2.00m $\times$ 2.62m. The two-dimensional hill and slope models whose profiles are those shown in Figure 1, and the span of 500mm were installed in the center of the tunnel test section of width 2.62m with endplates to improve two-dimensionality of the flow. The height $H$ of the model hill and the slope was 100mm. The on-coming flow of velocity $U_{ref}$ of approximately 8.0m/s was used so that the Reynolds number based on $U_{ref}$ and $H$ was fixed at $5.2 \times 10^4$. The mean and fluctuating velocity components were measured using a single-sensor hot-wire probe, with the sensor axis placed parallel to the boundary and normal to the free-stream direction. The instantaneous output could be related to the instantaneous velocity component normal to the sensor axis. The output of the hot-wire anemometer was digitized real-time and all the processing was done by a digital computer. The time average of the output could be related to the magnitude of the mean velocity, and the mean square as twice the turbulence kinetic energy $K$ if the lateral turbulence intensity could be estimated by the average of the other two intensities. The results, however, need to be interpreted with care, particularly in the region with instantaneous flow reversal, since the sensitivity to the velocity component parallel to the sensor axis is ignored. The measured results are shown together with the computational results in the following sections.

## 6. Properties of time evolution of the calculated results

Figures 4 and 5 show the contours of the instantaneous lateral vorticity distributions at a non-dimensional time interval of $\Delta t U_{ref}/H = 1.0$ calculated by the URANS and LES methods, for the flows over the isolated hill and over the ascending slope, respectively. It is seen that the URANS calculation results contain significant unsteadiness, particularly in the flow past a hill. They are not completely periodic, as would be expected of a phase-averaged quantity. In both isolated hill and ascending slope flows, the unsteadiness is initiated in the thin boundary layer near the top of the hill and grows into large-scale vortex structure downstream. These are definitely not the vortex-shedding type unsteadiness but are not quite the turbulent eddies, either. The LES results indicate, on the other hand, that irregular fluctuations appear somewhat downstream in the separated region, and they are more random with small-scale fluctuations superimposed on more vague large vortex structure. Other than these differences, the overall properties of both calculations share common features of filtered flow fields. There is no reason why the URANS results cannot be interpreted to represent a short-time average flow or laterally averaged flow. The results of the standard $k$-$\varepsilon$ method using a coarser grid and the wall-function boundary condition converged to a perfectly steady state after advancing for about ten non-dimensional time from an assumed initial condition of a uniform flow and showed no unsteadiness whatsoever.

## 7. Turbulent kinetic energy and eddy viscosity

Whether the unsteady fluctuations that have been seen in the URANS calculations are turbulence, or other type of motion including numerical instability, may be examined by looking at the kinetic energy of the computed unsteady fluctuations. Figures 6 and 7 show the calculated total kinetic energy:

$$K = \frac{1}{2}\left(\overline{\langle u_i\rangle\langle u_i\rangle} - \overline{\langle u_i\rangle}\,\overline{\langle u_i\rangle}\right) + \overline{\langle k\rangle} \tag{17}$$

compared with the experiments, the results of LES, and calculation using the standard $k$-$\varepsilon$ model for the hill and ascending-slope cases, respectively. Measurements were made by using the single-sensor hot-wire probe as described in the previous section, and the data shown here represent $1/2(\overline{u_1^2} + \overline{u_2^2} - \overline{u_1}^2 - \overline{u_2}^2$, which should correspond to the total turbulent kinetic energy $K$ when the lateral fluctuation is not significant. In the standard $k$-$\varepsilon$ calculation, there is no unsteady motion and $K = \langle k\rangle$. The average of the modeled part of the turbulent kinetic energy $\overline{\langle k\rangle}$ calculated by in the URANS is shown separately in Figure 8. It is seen that $\overline{\langle k\rangle}$ is one order of magnitude smaller than the total turbulent kinetic energy $K$. $K$ calculated by the present URANS agrees fairly well with the experimental $K$ and those calculated by the standard $k$-$\varepsilon$ method. It means that the difference between $K$ and $\overline{\langle k\rangle}$ should be the calculated part of the fluctuation, that is the quantity in the parentheses of equation (17). The LES results appear to show higher values of $K$ in the separated regions, which is predicted largest, but generally of similar order of

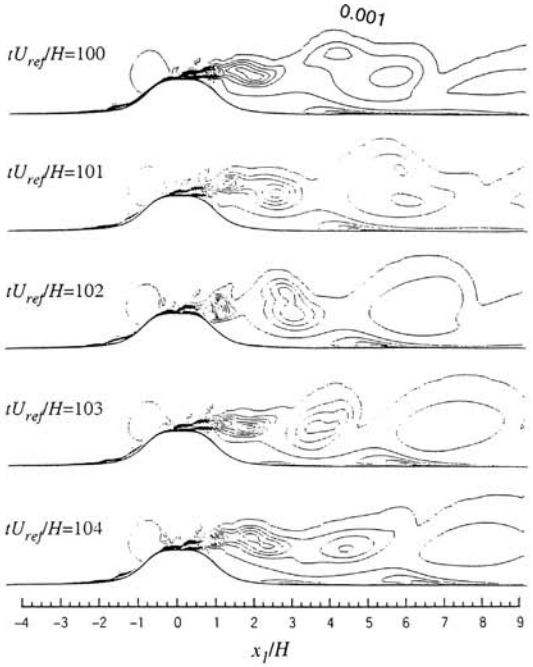


(a) URANS

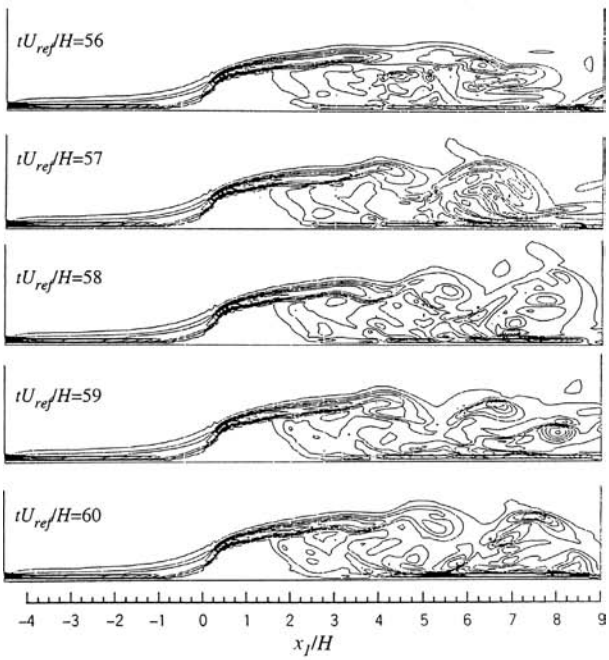


(b) LES

**Figure 4.**
Time development of lateral vorticity contours for isolated hill

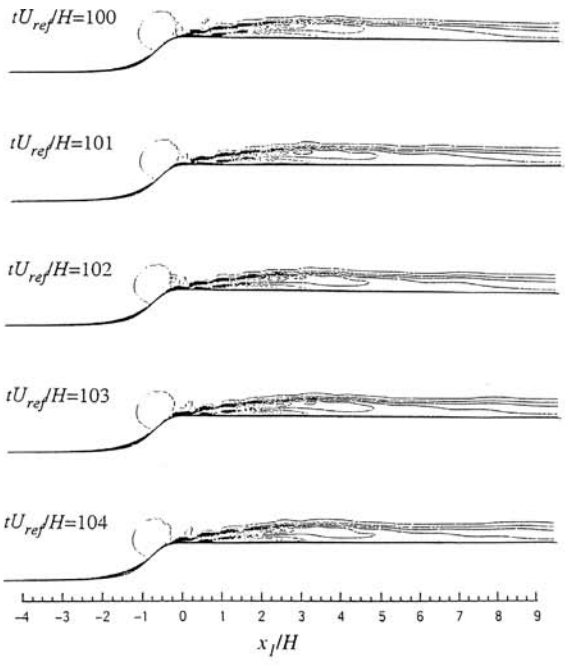


(a) URANS

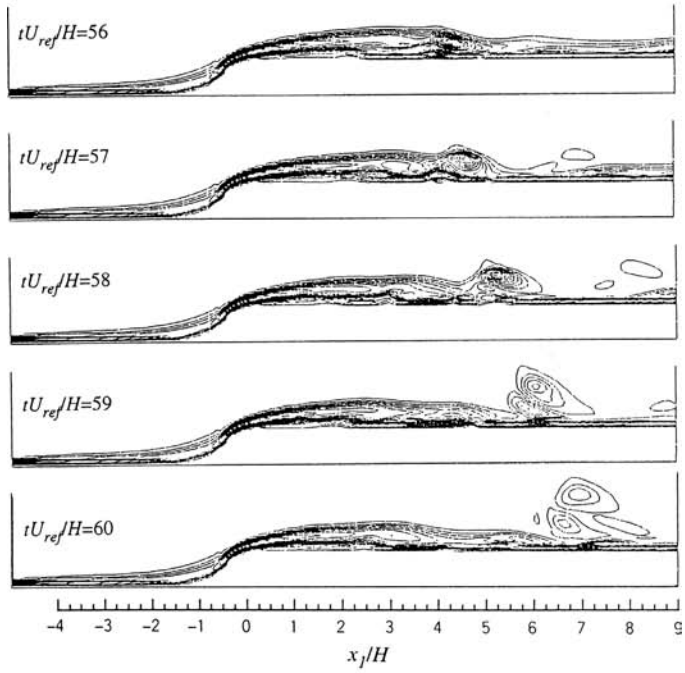


(b) LES

**Figure 5.**
Time development of lateral vorticity contours for slope flow

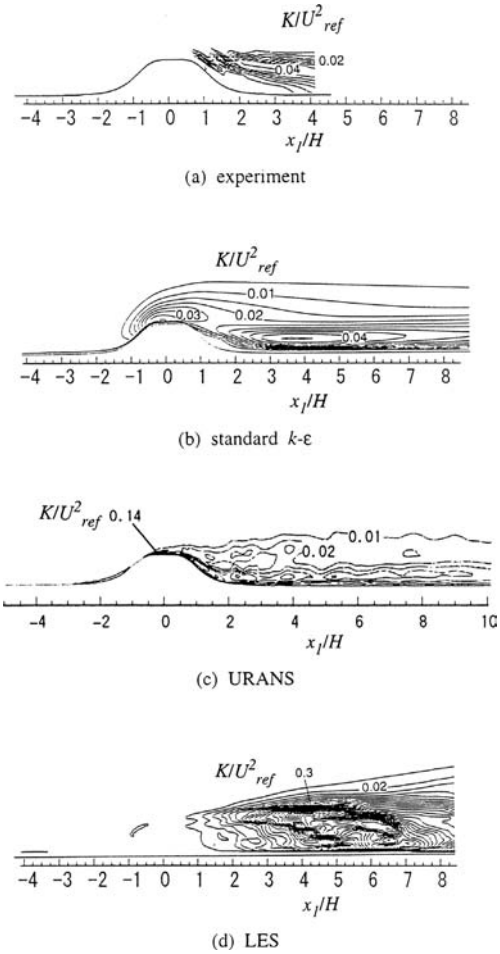


**Figure 6.**
Distribution of calculated total turbulence kinetic energy $K$ compared with experiments for the isolated hill flow

magnitudes with URANS. This indicates that the two-equation turbulence model used in the unsteady form computes the turbulence associated with the unsteady motion and is much like a simulation of filtered quantity. It seems that zero boundary condition for $\langle k \rangle$ and the near-wall damping of $\nu_t$ suppress generation of $\langle k \rangle$. Low $\langle k \rangle$ combined with the sufficient grid resolution work to generate small-scale motion that develops to the unsteady turbulent motion.

In order to see how the computed model parameters $\langle k \rangle$ and $\langle \varepsilon \rangle$ are associated with the unsteady motion, a sample of instantaneous distribution of the eddy viscosity $\nu_t$ in the case of isolated hill flow, is shown in Figure 9, together with the results obtained by the standard $k$-$\varepsilon$ method and the Smagorinsky model of LES. It is seen that $\nu_t$ distribution defined by $\langle k \rangle$ and $\langle \varepsilon \rangle$ in the URANS resembles that calculated by the standard $k$-$\varepsilon$ method in most of the flow away from the shear region downstream of the hill, though the position of the maximum is shifted somewhat downstream. The values in the

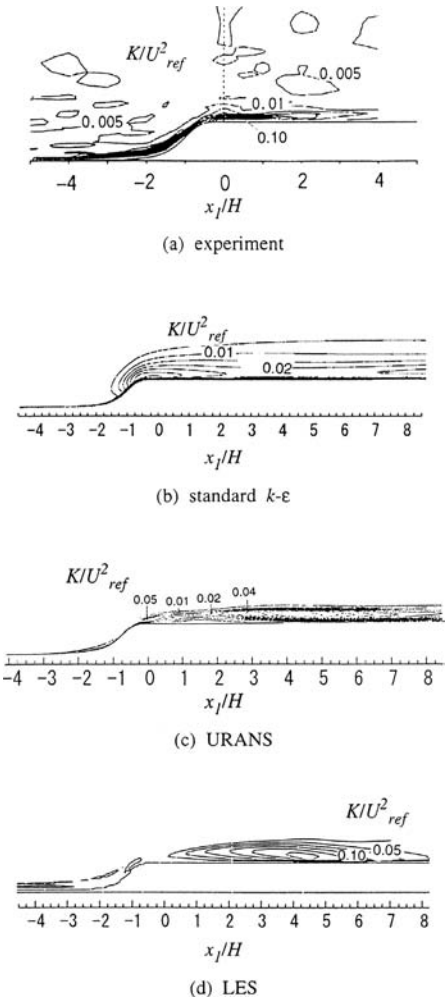


**Figure 7.**
Distribution of calculated total turbulence kinetic energy $K$ compared with experiments for the ascending slope flow

shear region and near the ground, however, are significantly smaller than in the rest of the region. This is the region where random turbulent motion exists. $\nu_t$ calculated by LES with the Smagorinsky model, on the other hand, takes significant values only in this shear region and very small in other parts. What should be noted is that values of the LES and those of URANS in the shear dominated turbulent region are about the same. This means that the flows calculated by both of these methods are similar in this region. In the region outside the shear region, URANS and the standard $k$-$\varepsilon$ model and Smagorinsky model show very different values of $\nu_t$. The former two show very large values, indicating effectively lower Reynolds number and more laminar-like flow there, while Smagorinsky model takes very small values. Whatever the reasons, these differences in these regions are not as important since there is not much turbulence there.

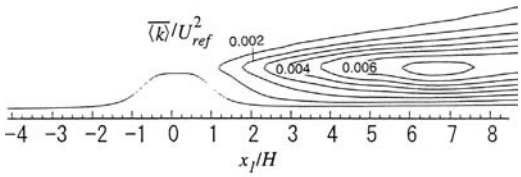


(a) isolated hill

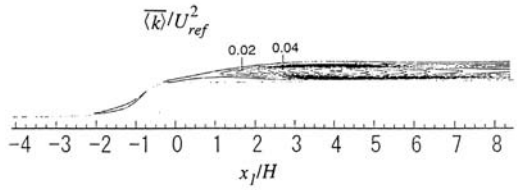


(b) ascending slope

**Figure 8.**
Distribution of the average of the modeled part $\langle k \rangle$ of turbulence kinetic energy calculated by URANS

## 8. Time variation and spectra of fluctuating velocity component

In order to further show what kind of fluctuations we are calculating, the time variations and the frequency spectra of a fluctuating velocity component at several positions in the flow are shown in Figures 10 and 11, respectively. The positions where velocity is sampled are shown in the top sketch of Figure 10. At the upstream station along the center of the hill, quite regular and fast oscillations are seen to be generated intermittently near the surface (point $A_3$), while there is only slow unsteadiness outside the boundary layer (point $A_1$). In the separated wake region, (points B's at $x/H = 2$ and C's at $x/H = 4$), there are no small oscillations and the fluctuations are seen to be very random with large magnitude near the surface. The large-scale fluctuation near the edge of the wake at point $C_1$ is seen to be negatively correlated with those at points near ground (point $C_3$) indicating an existence of a large vortex. At further downstream positions small-scale fluctuations are smoothed out and only large-scale fluctuations remain. These are all consistent with the properties of turbulent fluctuations expected in the separated flow woke the present one.

The power spectra of the fluctuating velocity components of Figure 10 are shown in Figure 11. It is seen that except for the point nearest the surface $A_3$, where a small peak exists corresponding to vortex shedding-like motion there, the spectra are very smooth. Also, except for points $A_2$ and $A_3$, the slope is slightly larger than but close to –3/5 in the range $0.1 < nH/U_{ref} < 1.0$, and steeper at higher frequencies. The calculation time step is $\Delta t = 0.0001 H/U_{ref}$, and the smallest grid spacing is $\Delta y = 0.007H$ which corresponds to the time increment of roughly $0.014 H/U_{ref}$ according to the Taylor hypothesis with the translation speed of $0.5U_{ref}$. Therefore, the limitation of resolving high-frequency motions is due to the insufficient grid spacing and the cutoff frequency is about $70U_{ref}/H$. The grid spacing at the sampling positions is two to ten times larger than this smallest spacing and the cutoff frequency is two to ten times smaller.

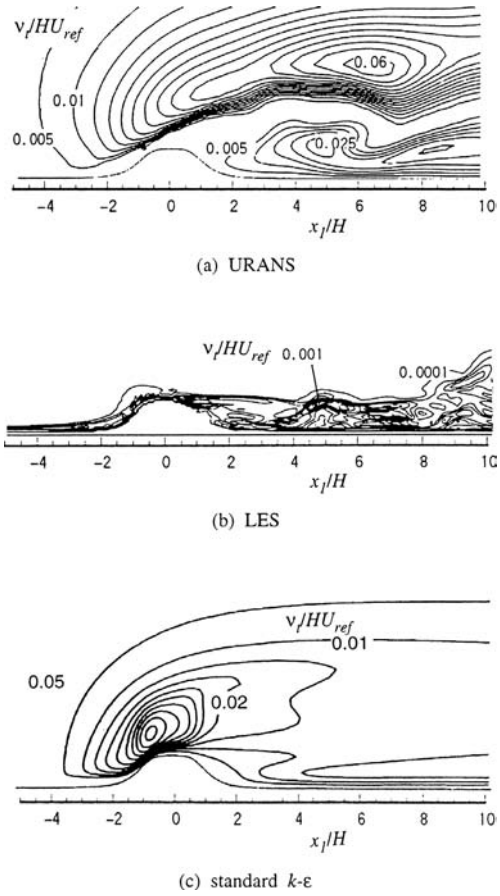


**Figure 9.**
Sample of instantaneous eddy viscosity coefficient $\nu_t$ for isolated hill flow

Considering the attenuation due to the insufficient spatial resolution, the spectra do show properties of filtered turbulent flow.

## 9. Mean velocity results

Figures 12 and 13 compare the magnitudes of the long-time averaged velocity $Q = \sqrt{(\langle\overline{u_1}\rangle)^2 + (\langle\overline{u_2}\rangle)^2}$ of the URANS and LES results and the average velocity $Q = \sqrt{\langle u_1\rangle^2 + \langle u_2\rangle^2}$ directly calculated by the standard $k$-$\varepsilon$ method as the steady-state values are compared with the experimental values $Q = \sqrt{(\overline{u_1})^2 + (\overline{u_2})^2}$. All of these are supposed to represent the same mean-velocity magnitude. It should be noted that $Q$ is always positive, even in flow reversing region. While the standard $k$-$\varepsilon$ method results appear to be closest to the experiments in terms of the size of the separated region and the shape of the contours, URANS results are seen to agree with both of these fairly well, indicating that the long time mean of the average velocity components $\overline{\langle u_i\rangle}$

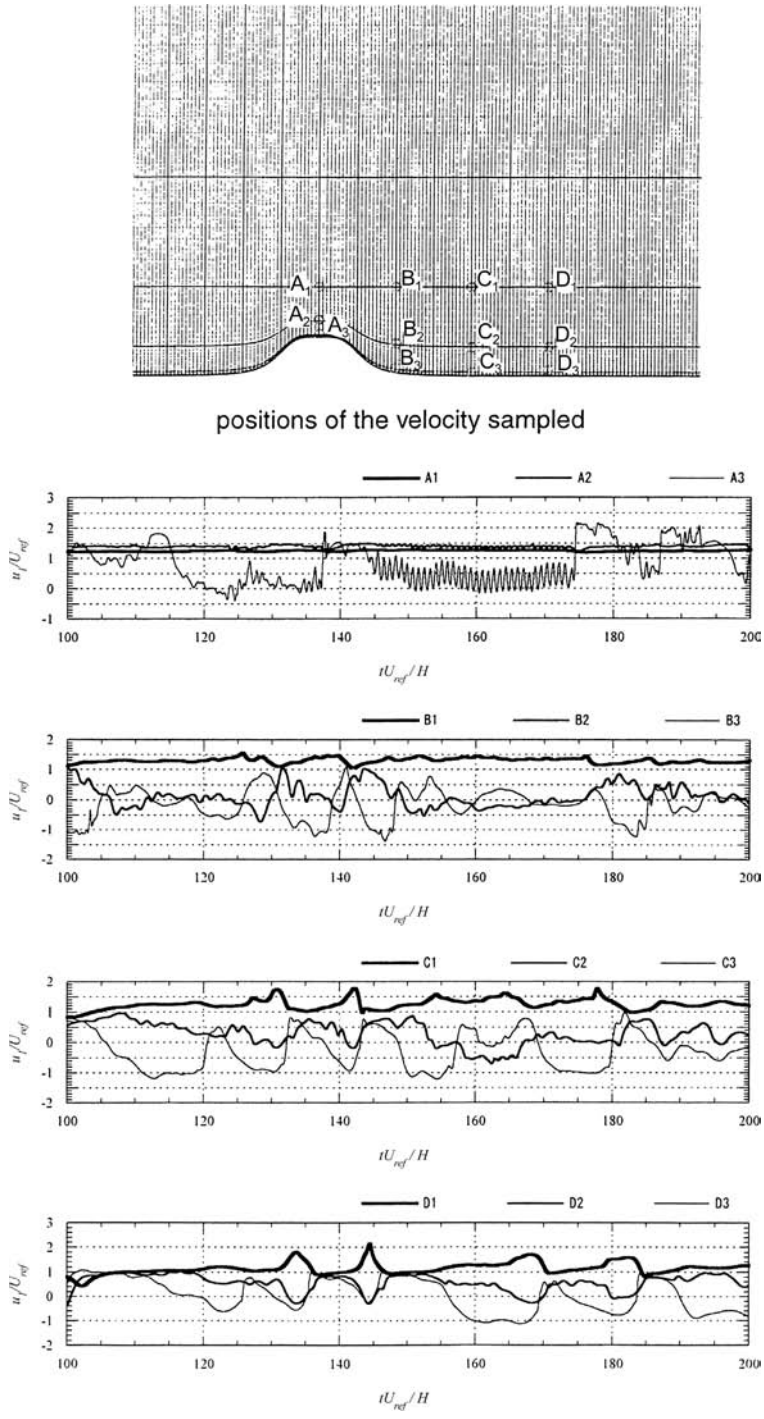


**Figure 10.**
Time variations of velocity component $u_1$ at selected positions

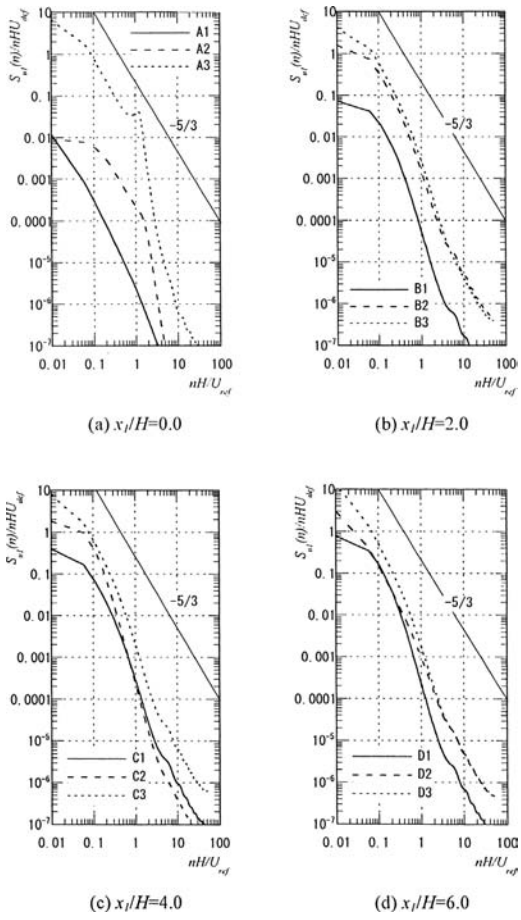


**Figure 11.**
Power spectra of fluctuating velocity component $u_1$ at the positions shown in Figure 10

correspond to the original Reynolds averages. Some waviness in the contours is seen at the flat surface on top of the hill over the ascending slope, which indicates that the randomness in the calculated results contains some consistent trend, but is expected to be due to insufficient computation time and is better than the separation predicted by the LES. Separate LES calculations were made with log-law boundary condition at the first calculation point from the ground, which showed improved mean velocity results but the turbulence was overly damped. Figure 14 shows comparisons of the mean velocity profiles, including the LES results with log-law boundary condition, at selected cross-stream sections. These indicate that calculations that use log-law boundary condition both the standard k-$\varepsilon$ and LES calculate the mean velocity profiles better. This is not because the log-law boundary condition is acceptable even in the separated region, but it is because the fully developed turbulence is assured if the log-law is used and the separation point is predicted more accurately. In the present URANS and LES with near-wall damping, there is no boundary layer tripping mechanism and the

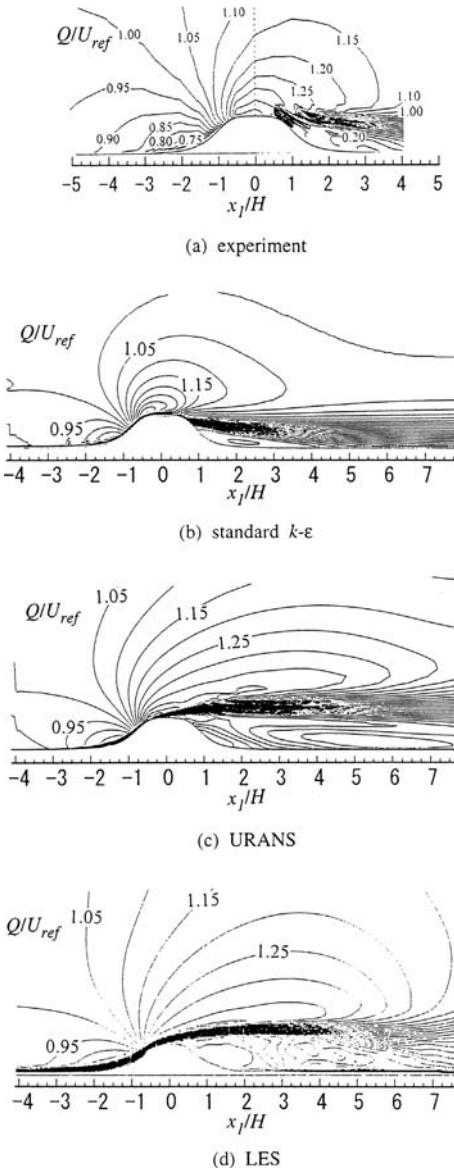


**Figure 12.**
Distribution of calculated mean total velocity $Q$ compared with experiments for the isolated hill flow

transition is not properly simulated in the upstream part of the flow. The profiles calculated by the URANS and LES without log-law at x1/$H$ = –2 indicate that the boundary layer is still laminar, which appears to be the reason for the early separation for the hill flow and separation in the case of LES for the slope flow. Therefore, the reason why the standard k-$\varepsilon$ method does well is mostly due to its correct prediction of the separation point, and does not undermine the accuracies of the present URANS.

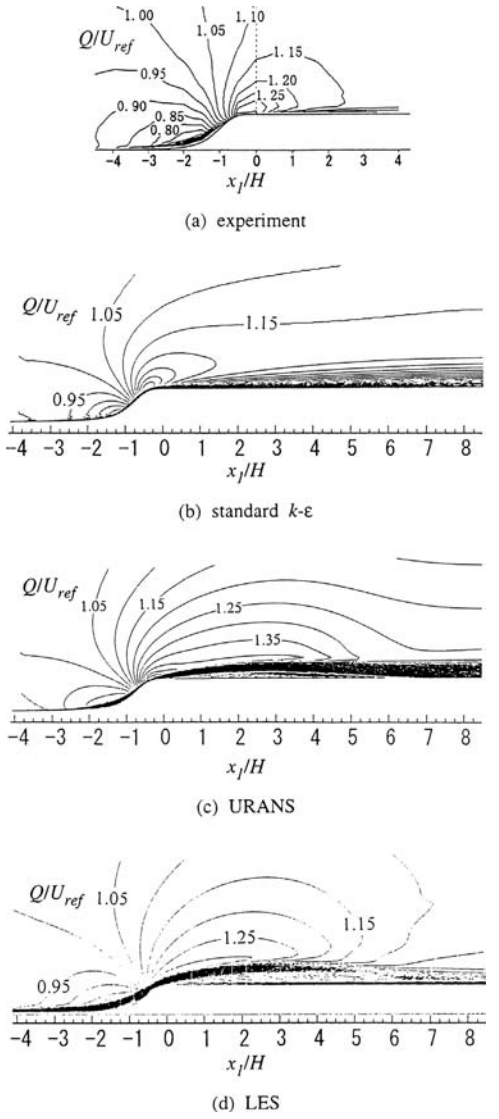


**Figure 13.**
Distribution of calculated mean total velocity $Q$ compared with experiments for the ascending slope flow

## 10. Discussion

The URANS and LES governing equations are formally the same. So there is no reason why one method must always produce a steady or deterministic periodic flows while the other obtains unsteady chaotic motions. The only difference lies in the meaning and the modeling of the eddy-viscosity coefficient if an eddy-viscosity model is used. If a two-equation model is used in the URANS, the eddy viscosity coefficient is given by the length and velocity scales inferred from the parameters that are calculated by their transport equations. On the other hand, if a conventional non-dynamic Smagorinsky

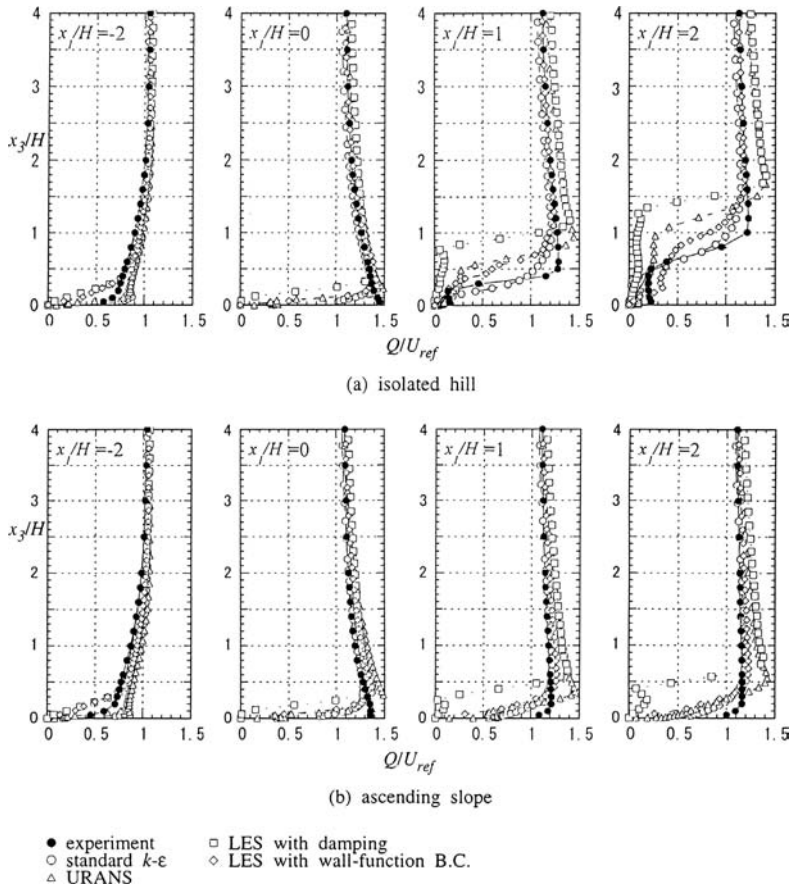


**Figure 14.**
Velocity profiles along selected cross stream sections

model is used in LES, it is fixed with the grid scale and the local rate of strain and it assures smaller stress for higher resolution. The main question now is what the calculated time-dependent flow represents in which the fluctuation energy $\langle k \rangle$ and its rate of dissipation $\langle \varepsilon \rangle$ satisfy the assumed unsteady transport equations and the empirical relations. The present calculations indicate that its long time average agrees remarkably well with both the steady conventional RANS results, and the experiments. Furthermore, the instantaneous results resemble the LES in many respects and though a theoretical explanation is not possible at the present stage, they appear to represent some kind of filtered flow field of which filter scale is implicitly built in the solution and not imposed by such factor as the grid spacing or time step of the numerical descretization. It means that an artificial ramp function that is used to bridge a RANS model to DNS depending explicitly on the grid size, proposed by Speziale (1998), or similar relation contemplated by Baggett (1998) and Germano (1999) are not necessary. It should be remembered that the grid size and the filter width are different (Reynolds, 1990). Different orders of accuracies used in descretization, for example, result in effectively different

filter widths for the same grid systems. So the filter width implicitly determined by the solutions of the modeled transport equations may be more desirable. What is intriguing is that those $\langle k \rangle$ and $\langle \varepsilon \rangle$ calculated with the same values of the model constants used in the original steady $k$-$\varepsilon$ model but with the proper damping in the low-Reynolds number region, give appropriate levels of $\nu_t$ for the stress $R_{ij}$ that produces such a random flow. Since the standard $k$-$\varepsilon$ model, which uses the wall-function boundary condition which sets $\langle k \rangle$ and $\langle \varepsilon \rangle$ at the fully-turbulent equilibrium values, did not produce unsteadiness at all, the near wall modeling is essential, though the present method may not be the only one. An implication is that the unsteady Reynolds averaged equations of motion with conventional turbulence closure with low-Reynolds number near-wall treatment appear to represent some of the real unsteady large-scale motion of turbulence, though further computations using other models may be necessary to find out the exact requirements for simulating turbulent motions. We have tried calculations making the eddy viscosity to explicitly depend on grid size and the local turbulence length scale (Miyashita & Nakayama, 2001) in such a way that the eddy viscosity becomes zero when the grid can resolve the Kolmogorov scale. The results show some improvements.

## 11. Conclusions

An URANS equation method has been applied to compute the flow over two-dimensional smooth topography with and without flow separation and compared with a conventional RANS, LES results and experiments. The URANS calculation with sufficient grid resolution near ground and an appropriate near-wall model has been demonstrated to reproduce much of the large-scale unsteadiness and some of the turbulent motion. Comparisons of the instantaneous results with conventional LES, and the long-time averages with the conventional RANS results and experimental results indicate that the computed flow appears to be some kind of filtered flow. The filter scale is not explicit but is implied by the obtained results. Without adjusting the model constants, the overall accuracy of the time-averaged quantities does not indicate an overwhelming improvement over the standard two-equation model, due mostly to an insufficient prediction of the position of the transition and hence the separation points, they exhibit a possible generalization to a new simulation technique, which may be further refined by using an optimized model constants and introducing grid-dependent length scales.

### References

Baggett, J.S. (1998), "On the feasibility of merging LES with RANS for the near-wall region of attached turbulent flows", Annual Research Briefs, Center for Turbulence Research, pp. 267-77.

Bosch, G. and Rodi, W. (1998), "Simulation of vortex shedding past a square cylinder with different turbulence models", *Int. J. Numer. Meth. Fluids*, Vol. 28, pp. 601-16.

Bouris, D. and Bergeles, G. (1999), "2-D LES of vortex shedding from a square cylinder", *J. Wind Eng. and Ind. Aerofyn.*, Vol. 80, pp. 31-46.

Franke, R. and Rodi, W. (1991), "Calculation of vortex shedding past a square cylinder with various turbulence models", *Proc. Eighth Symp. on Turbulent Shear Flows*, Munich, Germany, pp. 20-1-1–20-1-6.

Garuelle, B. and Ducros, F. (1999), "Towards unsteady simulation of separation of boundary layer", *Proc. 1st Symp. on Turbulence and Shear Flow Phenomena*, pp. 1155-60.

Germano, M. (1999), "From RANS to DNS: towards a bridging model", *Direct and Large-Eddy Simulation III*, Voke, P.R., Sandham, N.D. and Kleiser, L. (Eds), Kluwer Academic, London, pp. 225-36.

Iaccarino, G. and Durbin, P. (2000), "Unsteady 3D RANS simulations using $\nu^2$-$f$ model", Annual Research Briefs, Center of Turbulence Research, pp. 263-9.

Ishihara, T. (1999), "A numerical study of turbulent flow over a steep hill", *J. Wind Eng*., No. 79, pp. 167-8 (in Japanese).

Ishihara, T. and Hibi, K. (2000), "Numerical simulation of turbulent flow over a steep hill", *J. Wind Eng*., JAWE, No. 83, pp. 175-88 (in Japanese).

Kimura, I. and Hosoda, T. (1999), "3-D unsteady flow structures around rectangular column in open channels by means of non-linear $k$-$\varepsilon$ model", *Proc. 1st Int. Symp. on Turbulence and Shear Flow Phenomena*, Santa Barbara, CA, pp. 1001-6.

Koutmos, P. and Mavridis, C. (1997), "A computational investigation of unsteady separated flows", *Int. J. Heat and Fluid Flow*, Vol. 18, pp. 297-306.

Lakehal, D. and Rodi, W. (1997), "Calculation of the flow past a surface-mounted cube with two-layer turbulence models", *J. Wind Eng. And Ind. Aerodyn*., Vols 67/68, pp. 65-78.

Lee, S. (1997), "Unsteady aerodynamic force prediction on a square cylinder using $k$-$\varepsilon$-turbulence models", *J. Wind Eng. And Ind. Aerody*., Vols 67/68, pp. 79-90.

Miyashita, K. and Nakayama, A. (2001), "Numerical simulation of turbulent shear flow over two-dimensional smooth topography using unsteady RANS method", *J. Struct. Constr. Eng*., Architecture Institute of Japan, Vol. 541 (in Japanese), pp. 79-85.

Nakamura, S., Miyashita, K. and Noda, H. (1998), "Wind-tunnel tests of two-dimensional hill models formed by curved surfaces", Annual Report of the Wind Engineering Inc., Tokyo.

Nakayama, A. and Noda, H. (2000), "LES simulation of flow around a bluff body fitted with a splitter plate", *J. Wind Eng. and Ind. Aerody*., Vol. 85, pp. 85-96.

Nakayama, A. and Vengadesan, S. (2001), "Wall modeling for LES of high Reynolds number flow over gentle topography", submitted to *The 8th Symposium on Flow Modeling and Turbulence Measurements*.

Okajima, A., Kazumi, T. and Kiwata, T. (1998), "Experimental and numerical studies on flow past a three-dimensional hill", *J. of Applied Mechanics*, JSCE (in Japanese), pp. 625-32.

Reynolds, W.C. (1990), "The potential and limitations of direct and large eddy simulations", in *Whither Turbulence? Turbulence at the Crossroads*, Springer-Verlag, Berlin, pp. 313-43.

Rodi, W. (1993), "On the simulation of turbulent flow past bluff bodies", *J. Wind Eng. and Ind. Aerody*., Vols 46/47, pp. 3-19.

Shimada, K. and Ishihara, T. (1999), "Prediction of aerodynamic vibration of rectangular cylinder by $k$-$\varepsilon$ model, *J. Aerospace Engineering*, Vol. 12, pp. 122-35.

Shimada, K. and Meng, V. (1998), "Applicability of modified $k$-$\varepsilon$ model on the prediction of aerodynamic properties of rectangular cylinders with various elongated cross sections", *J. Structural Eng*., JSA (in Japanese), pp. 73-80.

Spalart, P.R. (1999), "Strategies for turbulence modeling and simulations", *Engineering Turbulence Modelling and Experiments*, Vol. 4, pp. 3-18.

Speziale, C.G. (1998), "Turbulence modeling for time-dependent RANS and VLES: a review", *AIAA J*., Vol. 36 No. 2, pp. 173-84.